Advanced Powder Technology 22 (2011) 226–235

Contents lists available at ScienceDirect

Advanced Powder Technology

journal homepage: www.elsevier.com/locate/apt

Original Research Paper

Analysis and DEM simulation of granular material flow patterns in hopper models of different shapes

R. Balevičius [a,*], R. Kačianauskas [b], Z. Mróz [c], I. Sielamowicz [d]

[a] Department of Reinforced Concrete and Masonry Structures, Vilnius Gediminas Technical University, av. Sauletekio 11, LT-10223 Vilnius, Lithuania
[b] Laboratory of Numerical Modeling, Vilnius Gediminas Technical University, av. Sauletekio 11, LT-10223 Vilnius, Lithuania
[c] Institute of Fundamental Technological Research, Polish Academy of Sciences, St. Pawińskiego 5b, 02-106 Warsaw, Poland
[d] St. J. Matejki 8, 15-351 Bialystok, Poland

ARTICLE INFO

Article history:
Received 12 July 2010
Received in revised form 16 November 2010
Accepted 6 December 2010
Available online 18 December 2010

Keywords:
DEM
Mass flow rate
Velocity distribution
Plane-wedged
Space-wedged
Flat-bottomed hoppers

ABSTRACT

By using the discrete element method (DEM) a comparison and observations on material flow patterns in plane-wedged, space-wedged, and flat-bottomed hopper were accounted for. Numerical results obtained by combining data of individual particles, statistical processing of particle assemblies and evaluation of the field variables provided the essential characteristics for different regimes of the discharge flow (within steady or unsteady state of flow) and the differences in differently shaped hoppers due to different microscopic inter-particle friction. For validation of the performed simulations, velocity patterns developed in three-dimensional flat-bottomed hopper containing 20,400 pea grains were also analysed. To represent the continuum by avoiding the local effects produced by the individual grains, the simulation results were focused on the mean velocity distributions with data smoothening. The effect of rolling resistance on granular material flow was also considered.

1. Introduction

Containers with a variety of shapes are widely used in industry for storage of granular materials. Comprehensive historical review on handling technologies and designed methodologies presented from the engineering point of view was given by Roberts [1]. Proper description of granular material involves flow mode patterns, arching, forming of the stagnant zones, variable density of the flowing material and some other phenomena which are related with the shape of the containers and play a very important role in reliable design of that material storage structures.

Theoretical understandings about the granular phenomena are largely empirical and many simplified analytical methods have been developed since a work of Janssen [2]. The continuum approach used in frame of the classical mechanics does not provide insight into behavior occurring at the scale of individual grain [1–3], since the flow is mainly subjected by the kinetics of individual grains within the hopper. On the other hand, a fundamental statistical theory is not available to describe a random walk of contacting particles.

Contrary to the continuum approach, the discrete element method (DEM) allows for a microscopic insight into granular material behaviour with tracing in time all dynamical parameters of particles, such as position of individual grains, their velocity, acceleration and acting inter-particle forces. Comprehensive review of theoretical developments focusing basically on particles interaction and link between discrete and continuum modeling is presented by Zhu et al. [4]. Because of numerical difficulties and time-expensive computations, the earliest developments were restricted to 2D numerical models and were devoted to plane and axi-symmetric hoppers. Probably, the first systematic study on the DEM application to the filling of silos was given by Holst et al. [5]. A summary on collaborative investigation of 16 research groups and the influence of various simulation details was presented by the authors of this paper. The latest developments on DEM simulations of granular flow in hoppers are described in the review paper by Zhu et al. [6] and by Kruggel-Emden et al. [7].

Majority of the reports about the investigations of container flows do not deal with the comparative analysis on material flow patterns for differently shaped hoppers. Actually, there is still a lack in literature a quantitative and systematic investigation in order to compare the outflow mass, its rate, and velocity distribution during material flow within differently shaped containers. In work by Goda and Ebert [8], authors chose a pyramidal hopper, silo with a hopper bottom, and a vertical-sided silo with a flat bottom for DEM analysis to analyze wall pressure, material flow zones during

* Corresponding author. Tel./fax: +370 5 2745225.
E-mail addresses: robertas.balevicius@vgtu.lt (R. Balevičius), rkac@vgtu.lt (R. Kačianauskas), zmroz@ippt.gov.pl (Z. Mróz), irena.sielamowicz@gmail.com (I. Sielamowicz).

0921-8831/$ - see front matter © 2010 The Society of Powder Technology Japan. Published by Elsevier B.V. and The Society of Powder Technology Japan. All rights reserved.
doi:10.1016/j.apt.2010.12.005

filling and discharge. A discharge time and the discharge flow rate were taken to be optimality criteria, while the discharge mass and the shape of the hoppers have been considered as design variables in DEM analysis by Balevičius et al. [9]. Comparison of flow behaviour of the conical concentric and eccentric hoppers and optimisation of their geometry is given by Ketterhagen and Hancock [10].

Cleary and Sawley [11] and Cleary [12] investigated and described progress in the area of industrial applications in 3D cases. In recent years, the simplified assumptions on the inter-particle contact models have been reexamined, with account for non-symmetric particle shapes sometimes simultaneously combined with rolling effects [6,11,13,14].

The motivation of the current analysis is to compare the main granular material flow patterns in 3D differently shaped hoppers. Firstly, by combining data of individual particles, statistical processing of particle assemblies and evaluation of the field variables, the observations on the outflow mass, its rate, and velocity distribution are provided for plane-wedged, space-wedged, and flat-bottomed hoppers. Secondly, as a verification of the results provided, the refined 3D flat-bottomed hopper is additionally considered to examine adequacy of the obtained velocity profiles to those computed by well known Nedderman and Tüzün's [15] kinematical model.

The gained observations could be implemented for revising or developing the continuum-based models. In particular, there were some results concerning granular behavior in the space-wedged hoppers [16], but the theoretical continuum-based model for predicting the outflow rate for the space-wedged hoppers is still missing [17].

2. Discrete element concept

The granular material is assumed to be composed of a set of N discrete spherical visco-elastic non-cohesive frictional particles. Geometry of the particle i ($i = 1, N$) is defined by the radius R_i with a specified grain size distribution and physical contact conditions. Physical properties of each particle are constant and defined by density ρ, elasticity modulus E and Poisson's ratio ν.

The deformation of particles is typically approximated by a representative overlap in the vicinity of the point of impact. Details for contact geometry model may be found in Balevičius et al. [18]. The motion of i-th particle at time instant t is described by the Newton's second law:

$$m_i \frac{\mathrm{d}^2 \mathbf{x}_i(t)}{\mathrm{d}t^2} = \mathbf{F}_i(t), \tag{1}$$

$$I_i \frac{\mathrm{d}^2 \theta_i(t)}{\mathrm{d}t^2} = \mathbf{T}_i(t), \tag{2}$$

where $\mathbf{x}_i$ and θ_i are vectors of position and orientation of the center of gravity, m_i is the mass and I_i is the inertia moment of the particle i ($i = 1, N$).

Vectors $\mathbf{F}_i$ and $\mathbf{T}_i$ acting at the centre of gravity of the particle i are as follows

$$\mathbf{F}_i = \sum_{j=1, j\neq i}^{N_c} \mathbf{F}_{ij} + m_i \mathbf{g} \tag{3}$$

$$\mathbf{T}_i = \sum_{j=1, j\neq i}^{N_c} \mathbf{T}_{ij} = \sum_{j=1, j\neq i}^{N_c} \mathbf{d}_{cij} \times \mathbf{F}_{ij} \tag{4}$$

Here, $\mathbf{F}_i$ presents the sum of inter-particle contact forces $\mathbf{F}_{ij}$ and gravity forces defined by the vector of gravity acceleration $\mathbf{g}$. The resultant torque $\mathbf{T}_i$ is defined analogously, while $\mathbf{d}_{cij}$ is the vector pointed from the centre of the particle i to the contact centre of the overlapped particles; N_c is the number of contacts.

The calculation of inter-particle contact forces is based on Hertz or Hooke's and the simplified Mindlin–Deresiewicz's contact models. The applied visco-elastic inter-particle contact model considers a combination of elasticity, damping and friction force effects. Assuming the small overlap, the contact between two material particles, is modeled by a spring and dashpot in both the normal and tangential directions and an additional slider in tangential direction. The inter-particle force vector $\mathbf{F}_{ij}$ describing contact between the particles i and j acts on the contact point and may be also expressed as a sum of the normal and tangential components $\mathbf{F}_{n,ij}$ and $\mathbf{F}_{t,ij}$, respectively. Rolling effects will be considered exclusively in Section 6. The normal component presenting, actually, repulsion force comprises elastic and viscous ingredients. The tangential component reflects static or dynamic frictional behaviour. The static force describes friction prior to gross sliding and comprises elastic and viscous ingredients, while the dynamic force describes friction after gross sliding and is expressed by Coulomb low.

The boundary conditions are determined by the walls treated as the planes of finite size. In their contact with particles, the walls are treated as rigid particles of infinite radius and mass. The particle–wall contact forces $\mathbf{F}_{ij}$ are therefore specified according to the inter-particle contact models in terms of the effective parameters. The effective radius of the contacting particles i and j is defined as $R_{ij}^{eff} = \left(\frac{1}{R_i} + \frac{1}{R_j}\right)^{-1}$. In the case of wall defined by $R_j = \infty$, it simply equals the radius of the particle, $R_{ij}^{eff} \approx R_i$. The remaining effective parameters such as mass, elasticity modulus, etc., are defined in the same manner.

Detection of the particle and the wall contact interaction is performed by creating locally oriented boundary cells and by checking the contact possibilities with the plane of the wall and its edges in the local coordinate frame. Modeling details were described in [19].

Details of the time integration procedure may be also found in [18,20]. Numerical simulations are obtained by using the developed original software *DEMMAT* by Balevičius et al. [21].

3. Granular material and hopper

As is well-known, the DEM simulation is highly time-consumable, mainly due to the contact searching procedure and a small time step required for correct integration of equations of the particles motion. To reduce the simulation time needed to model granular material flow, the simplifying assumptions are usually applied with respect to hopper shape, number and size of particles and material properties. It is a common practice to simplify computations, cf. [7,13].

The specified composition of granular material will be applied for investigating of bulk flow in differently shaped hoppers. It is represented by an assembly of $N = 1980$ particles. The values of the particle radii R_i ranging from 0.03 to 0.035 m are defined randomly with uniform distribution. Total mass M of the material is fixed and is equal to $M = 143.7$ kg. The data of the visco-elastic

Table 1
Major data of the particles.

Quantity	Symbol	Value
Density (kg/m^3)	ρ	500
Poisson's ratio	ν	0.30
Elasticity modulus (Pa)	E	0.3×10^6
Shear modulus (Pa)	G	0.11×10^6
Normal viscous damping coefficient (1/s)	γ_n	60.0
Tangential viscous damping coefficient (1/s)	γ_t	10.0

particle are given in Table 1. Inter-particle and particle–wall friction coefficient corresponds to the case of fully rough walls, while their values $\mu = 0 \div 0.6$ are simply assumed for modeling purposes. Note, a linear spring model based on Hooke's law is used for the normal contact.

Three differently shaped hoppers are investigated, while geometry of them is defined in the same manner (Fig. 1). The characteristic dimension of the outlet D is assumed to be related to the maximal diameter d of the particle as $D = 8.6d$. The thickness of the hopper at the bottom is assumed to be $B = 4.3d$. The dimension of the top hopper edge is $L = 3.3D$, while the overall height of the hopper is $H = 2.88D$. Assuming that $d = 0.06$ m, the main geometrical parameters of the hoppers are defined as: $B = 0.3$ m, $L = 1.6 \div 2$ m and $H = 1.7$ m.

Different shape is defined by inclination angles of the generetrix to the horizontal plane, θ_x and θ_y, respectively. The *space-wedged* hopper is described by acute angles having values $\theta_x = 68°$ and $\theta_y = 62°$, while values $\theta_x = 68°$ and $\theta_y = 90°$ correspond to the *plane-wedged* hopper. The *flat-bottomed* hopper is stated by assuming the right angles to be $\theta_x = 90°$ and $\theta_y = 90°$. Variable dimension of the bottom L_b depends on the hopper shape, however, dimensions of the outlet D and B are held constant, for all hoppers, for the sake of comparability. The hopper walls (including the bottom) are assumed to be rigid and are considered as the fixed boundaries with friction.

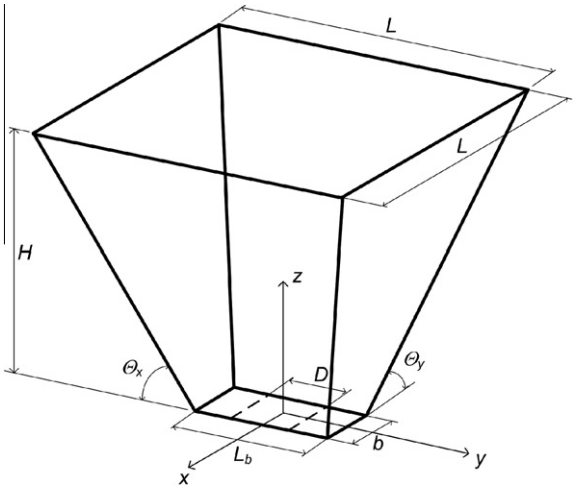

Fig. 1. The geometry of the hopper.

4. Illustration on the filling and discharge processes

Granular flow in hoppers is a continuous process, simulation of which may be considered in several stages reflecting different physical as well as technological aspects of this complicated phenomenon.

In the framework of current investigation, filling is considered as compacting of material for proper simulation of discharge. The filling is simulated by compacting the particles *en masse* i.e. all particles undergo the fall due to action of force of gravity and initial particle velocities imposed. A gradual filling procedures leads to a more fully developed internal and wall stress after filling due to better consolidation of the settled material [cf. 22,23]. A gradual filling was applied a further to simulation presented in Section 7. However, the filling procedure plays minimal effect on the discharge parameters.

During the particles settling on the bottom the orifice is kept closed until quasi-static state occurs. It corresponds to the average particle flow velocity equal to 10^{-7} m/s and practically negligibly

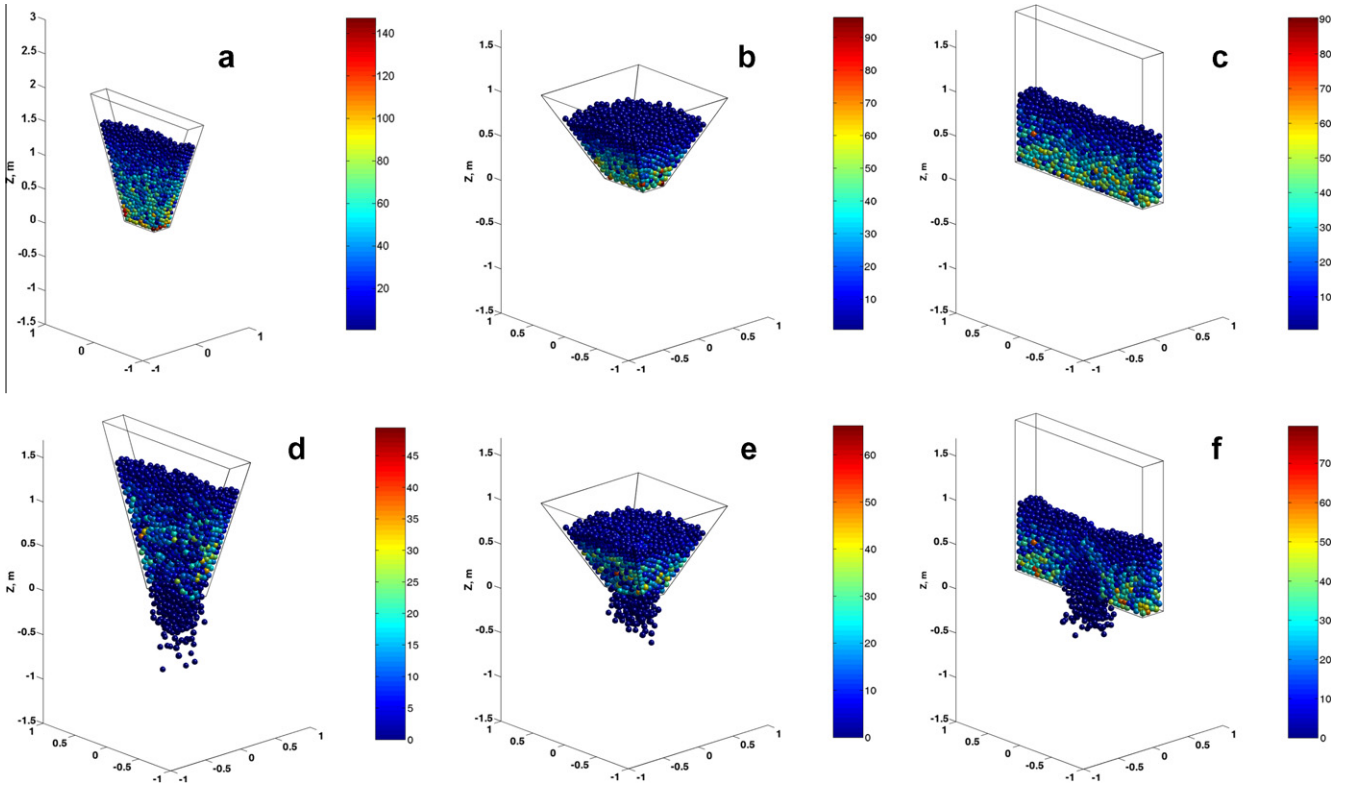

Fig. 2. Illustration of the discharge flow at various time instants ($\mu = 0.3$): (a and d) plane-wedged hopper; (b and e) space-wedged hopper; (c and f) flat-bottomed hopper; (a–c) the end of filling; (d–f) discharge process at $t = 0.4$ s. Color-bar indicates the particle contact forces measured in N (Newtons).

small average acceleration. The controlling indicator to achieve the quasi-static state was the total kinetic energy of granular material expressed as the sum of all particles energies due to translational and rotational motions.

The discharge process is simulated by instantly opening the orifice and allowing for free falling of the particles. Such a scenario of the emptying process presents an attempt to follow as close as possible the discharge stage encountered in real hoppers, if drawdown is not compensated by re-supplying the material from above.

A detailed description on the simulation aspects can be found in [18]. A specific scenario when the discharged particles are recycled back to the top of the hopper flow is used by Cleary and Sawley [11]. Such an approach is preferable for imposing the steady-state flow required, but differs from the discharge conditions in real hoppers.

Series of independent DEM simulations of the filling and discharge in three differently shaped hoppers were performed with different values of the friction coefficient but with the same above described composition of the granular material. Snapshots on the filling and discharge processes for differently shaped hoppers are summarized in Fig. 2. The colour-bar depicted in these figures shows the contact forces acting on the particles within the granular material. The color is specified by the scalar of $f_i = \sum_{i \neq j} |\mathbf{F}_{ij}|$ derived by summing up of inter-particles contact forces $\mathbf{F}_{ij}$ acting on the particle i.

The state of the rest, (Fig. 2a–c) illustrates variation of the individual particle contact forces within the bulk material which is exclusively governed by its own weight yielding lower values in the upper part of the hopper and higher values near the bottom.

Even simple examination of flow patterns allows identifying the important features of the discharge flow. Generally, for the case of fully rough wall, which immobilizes particle slipping downwards adjacent to the wall, the top surface of the material during the discharge transforms from a convex to a concave shape. This is quite illustratively exhibited in the case of *flat-bottomed* hopper (Fig. 2). In particular, the depression zone above the orifice occurs at the beginning of the emptying process. Later, this depression deepens with progressing of the emptying. Its sides become more and more steeper and when the slope of these sides reaches the angle of repose some of the particles cascade down to the central part of the material which moves faster. The nature of granular flow in the flat-bottomed hopper contains characteristic features of funnel flow.

The character of the discharge flow in converging, i.e. in *plane-wedged* and *space-wedged* hoppers is quite different. The formation of the depression zone at the top surface starts only when the granular material overpasses some height of the hopper. This zone quite evidently expresses the final stage of the discharge.

Decompression of granular material in the middle section of the hopper indicates significant reduction of the magnitudes of particle contact forces in the discharge time period (Fig. 2d–f). This feature clearly illustrates presence of the material dilation phenomena. It takes the place due to inter-particle friction which allows for material shearing with increasing in the porosity and, in turn, reducing in the particles contact forces. A detailed analysis on the evolution of the porosity fields by means of the particle contacts forces developed during discharge is given in [18,24].

5. Numerical results and observations

A comparative investigation on the main macroscopic parameters to understand how they affect the granular flow in terms of different shapes of the hopper is an important issue in development of the prediction approaches. In a framework of current investigation, numerical analysis comprises particle velocity patterns, discharge flow parameters, statistical processing of particle accelerations.

Let us consider the discharge flow patterns in terms of the discharged mass. A dimensionless variable, $0 \leqslant w_f \leqslant 1$, representing the discharged mass fraction is computed as the ratio of the discharged mass, M_d to the total mass, M. A discharged mass fraction rate, i.e., mass fraction flux, is obtained as a time derivative of the discharged mass fraction, $\mathrm{d}w_f(t)/\mathrm{d}t$.

Variations of the above defined dynamic discharge flow characteristics for hoppers of different shape and different inter-particle friction coefficients are presented in Fig. 4. The graphs depicted clearly indicate influence of the hopper shape and inter-particle friction. It can be also stated (Fig. 4d–f) that the highest discharged mass fraction rate occurs in the plane-wedged hopper, while in the space-wedged and the flat-bottomed hoppers discharge process runs in time relatively slowly. Plane-wedged hopper discharges faster than the space-wedged one, since, in the space-wedged hopper, the bulk flow exhibits *spatial retardation* due to an ability to generate more contacts with each other and dissipate the kinetic energy. For the plane-wedged hopper, *a plane flow* occurs only.

To discuss this in detail, let us analyze the polar plot of the particle horizontal velocities v_x and v_y developed at $t = 1$ s, in the plane-wedged and space-wedged hoppers during discharge. To this end, the horizontal velocities of the particles were plotted on a circular grid as the arrows emanated from the origin (Fig. 3).

As can be quantified by the polar plot (Fig. 3), the horizontal velocities v_x and v_y have almost isotropic distribution during discharge, for the space-wedged hopper. They maximal magnitude varies over 0.5–0.6 m/s. In the case of plane-wedged hopper, an anisotropic velocity distribution with domination of the component v_y is clearly observed. This component induces the particles movement toward the centre of the hopper with a twice higher velocity in comparison with the space-wedged hopper. Hence, for the space-wedged hopper an isotropic distribution of velocities leads to the ability of particles to get more contacts resulting in the space-retarded motion which reduces a vertical velocity produced by the gravity acceleration. Due to a space-retarded particles motion the space-wedged hopper discharges more slowly.

Generally, the discharge flow in the both space-wedged and flat-bottomed hoppers during the time interval up to 1 s behaves, in fact, quite similarly. At the beginning of discharge the non-linear

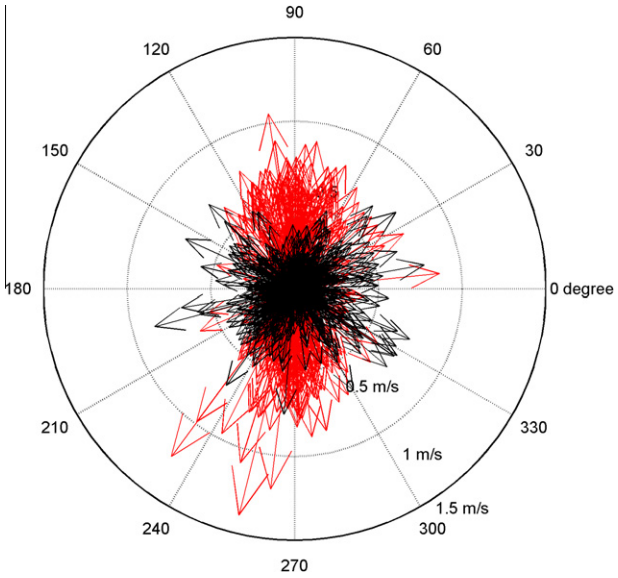

Fig. 3. Polar plot of particle velocities v_x and v_y on a circular grid, for the plane-wedged (red color) and space-wedged (black color) hoppers ($\mu = 0.6$).

variation between the discharged mass fraction with time is detected. This is due to formation of dilation wave which forms near the bottom and quickly spread over the whole material. Speed of propagation of this wave is dependent the inter-particle contact network and material damping and friction.

It could be also noted, that the flat-bottomed hopper cannot be completely discharged. Obviously, sequentially examining the flow rates we can see that increasing of the particle friction compared to the frictionless material induces diminishing of the discharged mass fraction rate. Generally, the influence of inter-particle friction coefficient, ranging from $\mu = 0.3$ to 0.6, is a quite mild and is invariant of the hopper shape, complying with a correction factor C used in theoretical prediction for the discharged mass rate. As pointed out by Nedderman [25], values of C as large as 0.64 have been reported for exceptionally smooth particles, while for frictional ones usually takes a value close to 0.58. Sometimes artificially established correction factor C serves as a remedy to fit the experimental values of the discharged mass rate with an experiment instead of new theoretical developments.

Important issue in continuum mechanics is the detection of steady state conditions. By generalization numerous empirical observations on the frictional granular material the main geometrical conditions defining the constant discharged mass rate have been established by Nedderman [25]: (a) the rate is independent of material height H, provided $H > 2D$; (b) the rate is independent of the orifice diameter, provided $L > 2.5D$, where L is shown in Fig. 1, as the width of the upper edge of the hopper.

Hence, the above statements provide that the particles theoretically accelerate freely and the main parameters affecting the flow rate are the bulk density, the orifice diameter and the inter-particle friction (irrespective to time-dependent analysis). For consideration of the frictionless materials, the inviscid fluid model defining the discharged mass rate of the fluid being proportional to $\sqrt{H}$ may be used for the sake of comparison.

By considering a variable material height in the space-wedged and flat-bottomed hoppers (Fig. 2), it is easy to persuade, the material height does not match the above geometric condition (a). Let us discuss the tendencies of the discharged mass fraction rate variation against the material height (Fig. 4g–i).

Thus, as expected, the discharged mass fraction rate of the frictionless particles (Fig. 4g) is similar to the above mentioned behavior of the fluids and seems to be proportional on $\sqrt{H}$, for geometrical configurations of the hoppers considered. For frictional particles, the discharged fraction rate should be theoretically independent on the quantity of material, typified by the height, H. This indication is fulfilled for the plane-wedged hopper very well within almost entire period of emptying. It means that, the discharged mass fraction rate could be effectively approximated by the

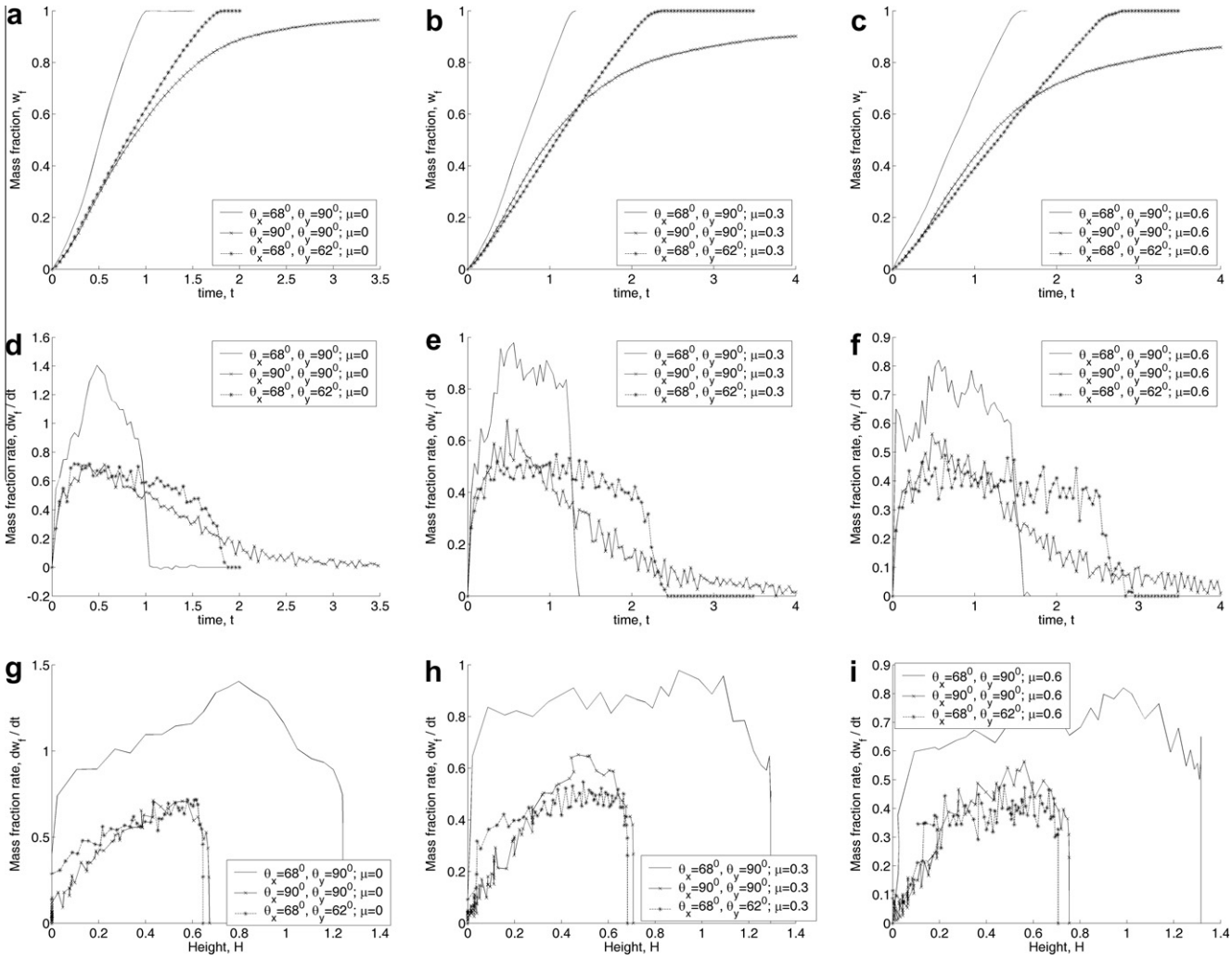

Fig. 4. Illustration of the discharge flow parameters in different hoppers for various inter-particle frictions: (a–c) time variations of the discharged mass fraction, (d–f) time variations of the discharged mass fraction rate, (g–i) variations of the discharged mass fraction rate against the material height. Parameters on axes dw_f/dt and H are measured in s^{-1} and m, respectively.

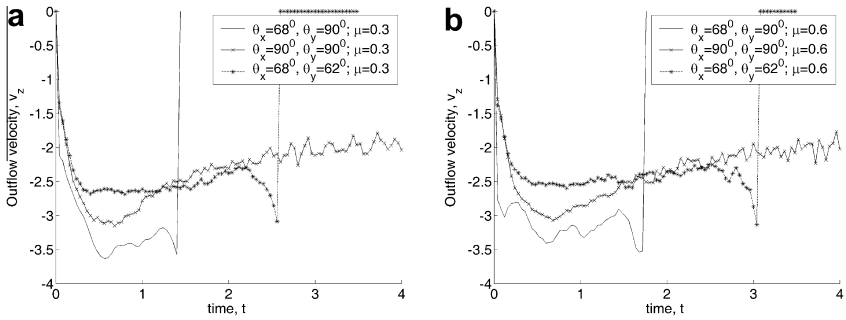

Fig. 5. The time variations of the vertical component of the average outflow velocity (measured in m/s) in different hoppers for different friction coefficients: (a) $\mu = 0.3$; (b) $\mu = 0.6$.

straight line, for 0.2 m < H < 1.1 m. However, for the case of the space and the plane-wedged hopper discharged mass fraction rate grows up from the beginning of the discharge until 0.2–0.4 s and just at this time instant the rate remains constant. Indeed, in the case of flat-bottomed hopper, the indication of the invariant rate with respect to the quantity of material is generally not valid due to the sufficiently low initial material height.

Time variations of vertical component of the average outflow velocity v_z in hoppers for different values of friction coefficient $\mu = 0.3$ and $\mu = 0.6$ are depicted in Fig. 5. The average outflow velocity was simply determined as the mean velocity of the particles located at D distance below the orifice. As can be seen in Fig. 5, the fastest flow generates in the plane-wedged hopper. Space-wedged hopper, in comparison to the plane-wedged one, is characterized by lower velocities and the longer discharge time. Increase of friction indicates a mild reduction in the outflow velocity magnitudes. Different durations of the discharge, i.e. residence time, are also clearly observed, because the higher particle velocity values result into shorter discharge durations.

This parameter may be additionally related with a steady/unsteady state condition. Steady or unsteady flow character may be specified by considering time variations of this velocity for different discharge flows. The graph (Fig. 5a) not only proves presence of fluctuations but also exhibits different flow character between differently shaped hoppers. Fluctuations in the outflow velocity may be partially caused by the arch formation at the location of by about 2D above the orifice [18]. A steady flow clearly prevails in the space-wedged hopper almost within the entire period of the emptying, where the velocities remain constant versus time. The unsteady inertial flow takes place during the entire period of the emptying in flat-bottomed hopper. The similar nature of the flow is also detected in the plane-wedged hopper containing, however, fluctuations.

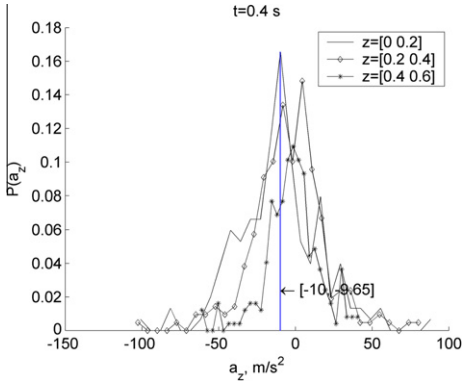

Fig. 6. The probability density functions for a vertical acceleration component of different layers in plane-wedged hopper.

The above investigation discovered that the most irregular random flow character occurs for the highest inter-particle friction, $\mu = 0.6$. In theoretical approaches, which are mainly devoted to flat-bottomed hoppers, the main assumption on the free acceleration of the particles near the orifice is employed. This assumption is sufficiently unclear for hoppers having the converging shape.

In order to verify the assumption concerning the state when the particles near bottom can accelerate due to gravity, the statistical analysis is employed (especially for converging shape of hopper). The discharged material is divided into separate layers, while three lowest layers defined by vertical coordinate intervals $z = [0, 0.2]$, $z = [0.2, 0.4]$ and $z = [0.4, 0.6]$ are considered. Each of the layers is characterized by probability density of the vertical acceleration a_z obtained by processing the values at various time instants. The characteristic simulation results are illustrated in Fig. 6, where variations of the probability density functions obtained for the plane-wedge hopper at time instants $t = 0.4$ s is presented.

As can be seen in Fig. 6, for $z = [0, 0.2]$, the peak of probability density function of vertical acceleration is obtained as close as the assumed range of acceleration due to gravity ($[-10, -9.65]$ m/s^2). This indicates that most of the particles near the bottom accelerate freely due to gravity. Meanwhile, a significantly lower pick of probability density function is obtained in the zones $z = [0.2, 0.4]$ m and $z = [0.4, 0.6]$ m where particles motion is sufficiently retarded due their acceleration/deceleration in the inter-particle contact collisions. Acceleration/deceleration of the particles may be attributed to the formation of series of linked stress arches (in our case at $z = [0.2, 0.4]$ m and $z = [0.4, 0.6]$ m zones) where above these arches the particles are packed together by retarding the flow and allowing to dominate gravitational fall at the vicinity of the bottom. For flat-bottomed hopper, the linked arches developed above the orifice were simply detected visually by plotting inter-particle contact forces web [18]. The experimental demonstrations of such arching and forces networking is presented by Poliquen and Gutfraind [26].

6. Some observations on the effect of rolling friction

The frictional forces usually induce the torques, so an additional influence of rolling friction may also be noticeable in reproducing the effects arising from the different physical factors during the rotational motion of the grains. In view of the existing results it could be stated that influence of rolling on the granular material behavior depends on the problem specified. A comprehensive review paper [4] lacks the data on rolling friction effects in hopper discharge. Consequently, some observations on this effect are demonstrated below.

Basically, the contact between two grains occurs not at a single contact point, but on a finite contact surface, and it is very difficult to fundamentally describe a contact traction evolution over this

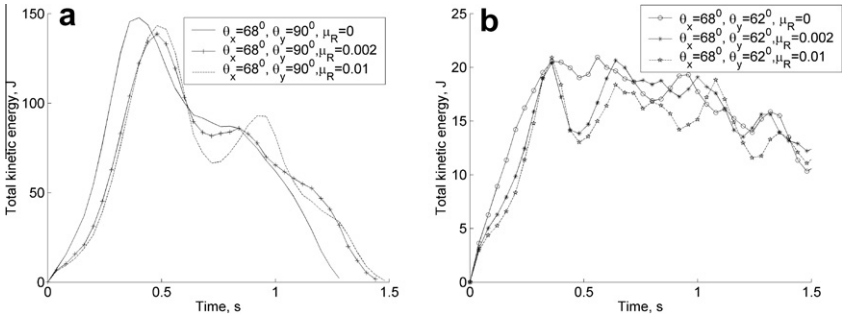

Fig. 7. Time histories of the system kinetic energy during discharge from the plane (a) and space-wedged (b) hoppers for various rolling friction coefficients μ_R = 0, 0.002, 0.01 (μ = 0.3).

surface [27,28]. However, a number of simplified approaches devoted to modeling the rolling resistance have been implemented in studies [29–33].

The rolling torque $\mathbf{T}_{ij}^{roll}$ always counteracts the relative rotation between two contacting entities manifesting the asymmetry of the normal traction distribution on the contact surface and causing a gradual slowdown in the rotational motion. Here, we determine $\mathbf{T}_{ij}^{roll}$ in terms of the approaches [13,14,31,32]. $\mathbf{T}_{ij}^{roll}$ can result from the torque supplied by the elastic spring which acts prior to the rolling or the torque originated during the rolling and modeled by a roller, thus:

$$\mathrm{T}_{ij}^{roll} = -\min\left(\left|k_r \frac{\int \omega_{ij}(t)\mathrm{d}t}{|\int \omega_{ij}(t)\mathrm{d}t|}\right|, \left|\mu_R r_{ij}|\mathbf{F}_{n,ij}| \frac{\omega_{ij}}{|\omega_{ij}|}\right|\right), \quad (5)$$

where $\omega_{ij} = \omega_i - \omega_j$ is the relative rotational motion at the contact centre resulted from the rotational velocities ω_i and ω_j for the particles i and j, respectively; k_r is the rolling stiffness [33], $r_{ij} = \min(R_i, R_j)$ is the effective radius of the contacting particles, $\mu_R = \tan(\alpha)$ is the coefficient of rolling friction provided by the tangent of the asperity contact angle α.

To analyze the effect of rolling friction on behavior of the granular material flow during the discharge process, the rolling torque $\mathbf{T}_{ij}^{roll}$ was added to the torque $\mathbf{T}_i$ in Eq. (2) and the subsequent flow analysis was performed. A suppression of rotation in opposite direction (due to rolling friction) at the full slowdown of the rotational motion was also considered during the numerical implementation.

In the experimental tests conducted for the spherical balls [34], values of the rolling friction coefficient have been found ranging mostly from 0.002 up to by about 0.013, depending on the material used. In the current investigation, three limiting values of $\mu_R = 0$, 0.002 and 0.01 were roughly selected to evaluate the effect of rolling friction on bulk flow. Meanwhile, the total kinetic energy, presented as a sum of the translational and rotational kinetic energies of individual particles, is considered as a main indicator. The evolution of total kinetic energy during the discharge process for the particles inside the hopper is presented in Fig. 7, for the plane and space-wedged hoppers.

In Fig. 7, the depicted graphs actually indicate the increase in total kinetic energy for the case of $\mu_R = 0$, for both hoppers. This increase is essentially produced by the rotational energy, since the particles without rolling friction have a higher capability to rotate during discharge. This effect dominates at the first 0.5 s of the discharge process, when an increasing quantity of material within the hopper is able to induce the bulk flow. Later, when amount of the particles inside the hopper decreases (roughly up to 50%, cf., Fig. 4 b), the motion of individual grains can contribute even to a slight increase in the total kinetic energy for model possessing the rolling friction. Notably, the differences between the total kinetic energy evolution are sufficiently small, for the models with $\mu_R = 0.002$ and $\mu_R = 0.01$.

Thus, the selected interval of $\mu_R \in [0.002,\ 0.01]$ is not expected to take a large affect on bulk flow characteristics, and rather, the other material parameters, such as the sliding friction, have a more significant effect during the discharge process. This also indirectly confirms the default value of $\mu_R = 0.01$ used by the commercial DEM software (EDEM™, DEM Solutions, Edinburgh, Scotland). However, the presence of rolling friction is expected to be a required and reasonable attribute to reproduce the experimental discharge behavior of granular material for the elongated irregularly shaped particles [14].

7. Adequacy of the numerical results to continuum prediction

To validate the above demonstrated simulations, their results should be verified with the continuum-based predictions. For space-wedged hopper, any theoretical prediction of the outflow mass rate is missing in literature. Meanwhile, verification of the obtained outflow mass and that produced by a well known Rose–Tanaka empirical formula was done in [18], for the plane-wedged hopper. Similar analysis relying on Baverloo's equation was presented in [24], for flat-bottomed hopper.

Hence, an adequacy of the numerically obtained velocity profiles to those computed according to Nedderman and Tüzün [15] kinematical model is rigorously checked here, for the flat-bottomed hopper.

To this and for proper representation of the continuum, the number of particles, representing the granular matter, was increased up to 20,400 grains. As distinct from the above artificially assumed properties of the particles, the pea grains were used. Also, the Hertzian spring is applied. Moreover, the experimental model was also constructed.

The model was composed of a flat-bottomed rectangular hopper made of Plexiglas and the rectangular in cross-section

Table 2
Main data on the pea grains.

Parameters	Quantity (mean ± st.dev.)	Explications and references
Particle elasticity modulus (MPa)	236.09 ± 40.89	Measured experimentally by compressing the grain between two plates
Restitution coefficient (particle–wall)	0.56 ± 0.12	Determined experimentally by the drop/rebound of the grain on the plexi plate
Friction coefficient (particle–particle)	0.29 ± 0.09	[35]

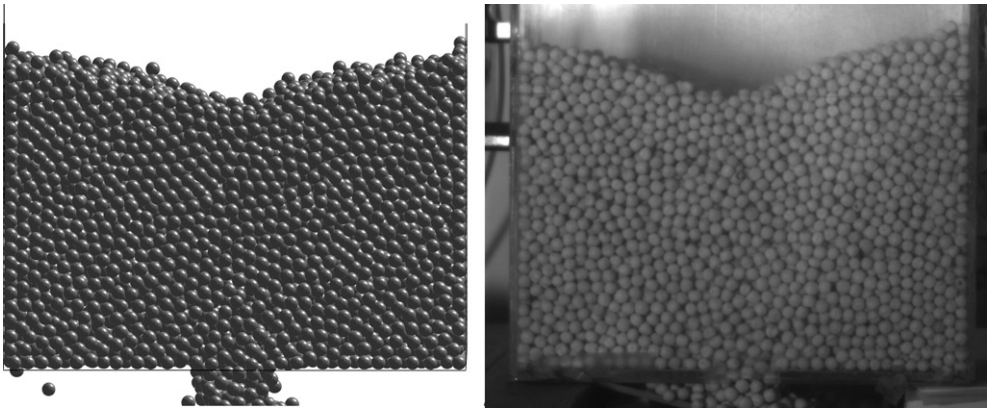

Fig. 8. Simulation and experimental snapshots of material flow.

container with a pyramidally adjusted bottom fabricated from cardboard. The container was installed on the hopper and basically served for filling of the material into the hopper. Hopper model had the following inward dimensions: height of 800 mm, width of 252 mm, and thickness of 108 mm. The width of outlet was of 42 mm.

The pea grains were simply poured into container. Measurements were taken when outlet of the container was opened and continued prior to opening outlet of the hopper, i.e. under the quasi-static conditions, as well as during the discharge when material flowed throughout the hopper's outlet.

The pea grains with the total mass of 5.87 kg had the diameter varying over the range of 7.2–7.8 mm and the particle average density of 1290 kg/m^3 (moisture content of 9%). The main micro properties of the particles used in the simulation are given in Table 2 relying on [35,36].

Simulation and experimental snapshots are depicted in Fig. 8. A detailed description on the peculiarities of the simulation can be found in [37,38]. As can be seen from these snapshots, the numerically obtained composition of the flowing material is very similar to that generated in the experiment. A sufficiently good match was observed during the steady flow conditions. At early phase and at the end of the discharge process some difference in material compositions was discerned. During these phases the flow is greatly affected by the dynamics of individual grains, and this effect vanishes when flow becomes steady.

The experimental measurement of the outflow rate and comparison with the numerical prediction could be found in [37] by the readers, while comparison of the experimentally measured wall pressures with simulation was given in [38].

Now, let us consider here a derivation of the continuum representative velocity profiles developed within the hopper during the material discharge. Velocity of individual grains traced during the DEM analysis cannot properly represent the continuum (cf., [39]).

Hence, to avoid the local effects produced by the individual grains, the simulation results should be focused on the mean flow parameters of the contacting particles. For this propose, the whole domain of the material was divided into the representative spheres. Detection of the particle within the representative sphere was simply defined relying on the positions of centre of the particle and the representative sphere and its radius. Spheres were regularly arranged with or without the overlap in order to fulfill the geometry of the hopper. In the following, the particles found within these spheres were identified at a certain initial time, and the identified particles were taken for the subsequent time instant to find the average velocity. The average velocity for sphere k was processed as follows

$$\langle \mathbf{v}_k(t+\Delta t)\rangle = \frac{\langle \mathbf{x}_k(t+\Delta t)\rangle - \langle \mathbf{x}_k(t)\rangle}{\Delta t}, \tag{6}$$

$$\text{where } \langle x_k\rangle = \frac{1}{n}\sum_{i=1}^{n} x_i, \langle y_k\rangle = \frac{1}{n}\sum_{i=1}^{n} y_i, \langle z_k\rangle = \frac{1}{n}\sum_{i=1}^{n} z_i, \quad (k=1,2,\ldots m) \tag{7}$$

are the averaged positions of the particles in the sphere k at a certain time, while x_i, y_i, z_i are vector $\mathbf{x}_i$ components for the particle i within the sphere k; n is number of the particles within the representative sphere, and m is number of the representative spheres.

The mean velocity vector components determined by using the above relationships are plotted in Fig. 9. The averaging process was performed by specifying the representative spheres having the size equal to 7–8 times of the largest diameter of the particle. Finally, the computed volumetric data for the velocity vectors (Fig. 9 a) are displayed on the spatial mesh by implementing cubic interpolation/extrapolation procedure. Implementation of this technique allows estimating the unknown values of the velocity components that lie between a probe's point of the representative spheres, as well as providing the continuity and the smoothness of the results obtained (Fig. 9 b). As can be seen in Fig. 9a, the averaging procedure performed produces the regularly distributed velocity vectors being in accord with the classical macroscopic description of the discharge flow for flat-bottomed hopper. It should be noticed; however, that some points located near the walls are matched with some errors resulted from the extrapolation procedure covered by a spline function.

Nedderman and Tüzün's [15] continuum kinematical model provides a sufficiently accurate prediction of the velocity profiles using only one unknown constant, for the convergent flow region under steady state conditions. It is assumed that the horizontal velocity is proportional to the gradient of downward velocity v_3 (i.e., a shear rate). Application of this assumption for an incompressible material yields [15]:

$$\frac{\partial v_3}{\partial z} = -b\frac{\partial^2 v_3}{\partial y^2}, \tag{8}$$

where y is the horizontal distance from the vertical axis of the silo, z is a distance above the outlet, b is the proportionality factor or diffusion length referred to by Choi et al. [40].

A Gaussian function fulfils the solution of (8), for v_3 and v_2 [15].

$$v_3(y,z) = \frac{Q}{\sqrt{4\pi bz}} e^{\left(\frac{-y^2}{4bz}\right)}, \tag{9}$$

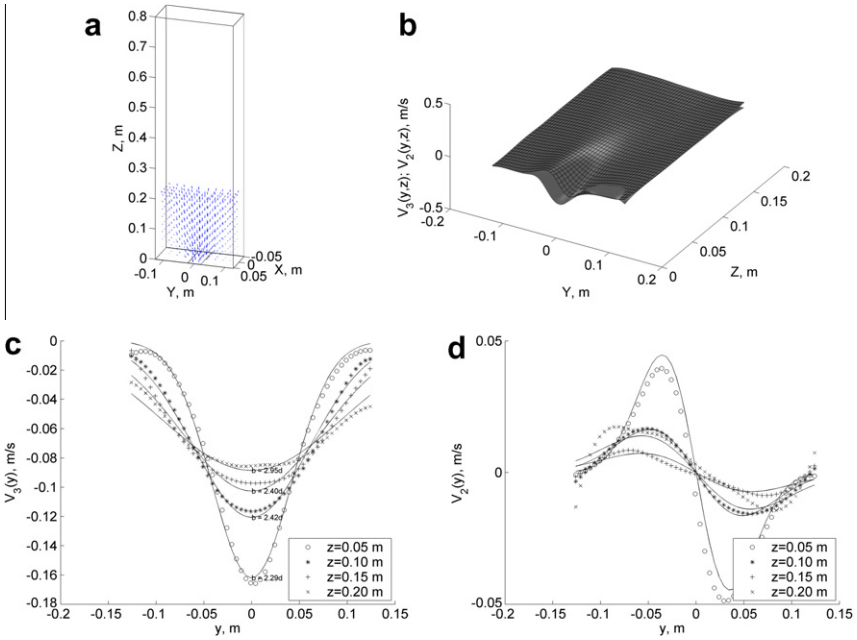

Fig. 9. Continuum representative velocities during discharge (t = 1s): (a) vector patterns; (b) vertical v_3 (gray color surface) and horizontal v_2 (meshy surface) velocity functions derived at the midsection plane of the hopper; (c) comparison with continuum prediction for vertical velocity; (d) the same for horizontal component.

$$v_2(y,z) = -b\frac{\partial v_3}{\partial y} = \frac{Q}{\sqrt{4\pi bz}}\frac{y}{2z}e^{\left(\frac{-y^2}{4bz}\right)}, \tag{10}$$

where Q denotes a volumetric flow rate per unit thickness of the silo, $v_3 \equiv v_z$, $v_2 \equiv v_y$.

Indeed, there seems to be no way to predict b a priori and the model cannot directly be applied as a predictive approach. However, to produce the observed velocity patterns (Fig. 9 b) we can adopt regression analysis for a suitable choice of b. Thus, denoting the first term of (9), as the downward velocity at the hopper centre line, $v_3(0,z) = \frac{Q}{\sqrt{4\pi bz}}$, we use a non-linear least square fit to find $v_3(0,z)$ and b in terms of the velocity patterns (Fig. 9 b). This simply allows for omitting the derivation of Q from the mass flow rate with respect to porosity evolution.

Distribution of the computed vertical velocity $v_3(y,z)$ (Fig. 9 b) clearly indicates a dominant plug flow with velocity maxima at the centre of the hopper and the stagnant zones developed adjacent to the walls. Graphs depicted in Fig. 9c show good agreement between the simulation and the fitted curves of Eqs. (9) and (10). As can be seen, the diffusion length b becomes larger when z increases in accord with some previous experimentally-based reports [25,40,41]. The obtained parameter b also confirms the condition of $b > d$ (d is the mean diameter of the particles) proving Litwiniszyn's [42] stochastic model, where b was treated as a hypothetical cage to replace a random walking particle. The values of b to obtain the best fit for the velocity profiles increases from $2.29d$ to $2.95d$ (Fig. 9c) replicating the experimentally found values. For example, Tüzün and Nedderman [15] experimentally determined that $b \approx 2.3$–$3.0d$ for various particle sizes, Kafui and Tornton [44] using DEM stated, $b \approx 2.7d$, Mullins [43] $b \approx 2d$ for iron ore particles, while Medina et al. [41] found that diffusion length varies from $b \approx 1.5d$ up to $\approx 4d$. In work [45], Nedderman and Tüzün's model was theoretically extended to account for eccentric discharge in a 2D flat-bottomed hopper.

In summary, the approach averaging the particle-level velocities to found their continuum-based equivalent enabled us transmitting 3D kinematical model to its planar equivalent [15]. Tuzun's kinematical model fitting to the averaged velocity values and comparison of the obtained values for the diffusion length with their equivalent covered in literature seems to be a reasonable way to evaluate the averaging technique.

8. Concluding remarks

The performed numerical modeling of filling and discharge processes in plane-wedged, space-wedged and flat-bottomed hoppers illustrated the potential of the DEM to understand and reproduce the complex flow of granular material. Numerical results obtained by combining the microscopic data of individual particles, statistical processing of particle assemblies and evaluation of the field variables provided the essential characteristics for different regimes of the discharge flow (within steady or unsteady state of flow) and the differences in differently shaped hoppers due to different microscopic inter-particle friction. The obtained observations could be implemented for revising and developing the continuum models, particularly for the space-wedged hoppers.

In particular, space-wedged hopper, in comparison to the plane-wedged one, is characterized by the lower outflow velocities and the longer discharge time. The plane-wedged hopper discharges faster than the space-wedged one due to the plane flow, while, the space-wedged geometry produces a space-retarded flow, where the particles have more abilities to dissipate kinetic energy by the contacts. In particular, an isotropic distribution of velocities for the space-wedged hopper leads to the ability of particles to get more contacts resulting in the reduced vertical velocity due to the gravity acceleration. For the plane-wedged hopper, an anisotropic velocity distribution with domination of the vertical velocity component was clearly observed. This component induces the particles movement toward the centre of the hopper with almost twice higher velocity magnitude in comparison with the space-wedged hopper.

Despite a small number of particles used the obtained results are quite representative and observations comparable with the continuum-based indications. The introduced rolling friction ($\mu_R \in [0.002\ 0.01]$) suppresses a local spin of the particles

decreasing their rotational abilities and rotational kinetic energy; however, the other parameters, such as, sliding friction, hopper shape have a more significant effect on the material bulk flow patterns.

It could be stated that the obtained DEM results are comparable with the continuum-based indications. The DEM produced velocity profiles in the 3D flat-bottomed hopper are adequate to those determined by using the Nedderman and Tüzün's kinematical model. The diffusion length values of the theoretical model are found to be in a good agreement with those reported in literature. These values also confirm the hypothetical cage size to replace a random walking particle according Litwiniszyn's stochastic model.

References

[1] A.W. Roberts, Particle and bulk solids handling technology – bridging the theory practice gap, in: Proceedings of World Congress on Particle Technology WCPT-5, CD-ROM, pp. 1–38. Orlando (2006).

[2] H.A. Janssen. Versuche über Getreidedruck in Silozellen. Z. Ver. Dtsch. Ing. 39(35) (1895) 1045–1049.

[3] H.M. Jaeger, S.R. Nagel, R.P. Behringer, Granular solids, liquids, and gases, Reviews of Modern Physics 68 (4) (1996) 1259–1273.

[4] H.P. Zhu, Z.Y. Zhou, R.Y. Yang, A.B. Yu, Discrete particle simulation of particulate systems: theoretical developments, Chemical Engineering Science 62 (2007) 3378–3396.

[5] J.M.F.G. Holst, J.Y. Ooi, J.M. Rotter, G.H. Rong, Numerical modeling of silo filling: II. Discrete element analyses, Journal of Engineering Mechanics 125 (1999) 104–110.

[6] H.P. Zhu, Z.Y. Zhou, R.Y. Yang, A.B. Yu, Discrete particle simulation of particulate systems: a review of major applications and findings, Chemical Engineering Science 63 (2008) 5728–5770.

[7] H. Kruggel-Emden, S. Rickelt, V. Scherer, A numerical study on the sensitivity of the discrete element method for hopper discharge, Journal of Pressure Vessel Technology 131 (2009) 031211.

[8] T.J. Goda, F. Ebert, Three-dimensional discrete element simulations in hoppers and silos, Powder Technology 158 (2005) 58–68.

[9] R. Balevičius, R. Kačianauskas, Z. Mróz, I. Sielamowicz, Discrete element method applied to multiobjective optimization of discharge flow parameters in hoppers, Structural and Multidisciplinary Optimization 31 (2006) 163–175.

[10] W.R. Ketterhagen, B.C. Hancock, Optimizing the design of eccentric feed hoppers for tablet presses using DEM, Computers and Chemical Engineering 34 (2010) 1072–1081.

[11] P.W. Cleary, M.L. Sawley, DEM modelling of industrial granular flows: 3D case studies and the effect of particle shape on hopper discharge, Applied Mathematical modelling 26 (2002) 89–111.

[12] P.W. Cleary, Industrial particle flow modelling using discrete element method, Engineering Computations 26 (6) (2009) 698–743.

[13] C. González-Montellano, F. Ayuga, J.Y. Ooi, Discrete element modelling of grain flow in a planar silo: influence of simulation parameters, Granular Matter, doi:10.1007/s10035-010-0204-9.

[14] D. Markauskas, R. Kačianauskas, Investigation of rice grain flow by multi-sphere particle model with rolling resistance, Granular Matter, doi:10.1007/s10035-010-0196-5.

[15] R.M. Nedderman, U. Tüzün, A kinematic model for the flow of granular materials, Powder Technology 22 (1979) 243–253.

[16] R. Balevičius, R. Kačianauskas, V. Vadluga, Investigation of three-dimensional granular stresses in pyramidal container after filling, Mechanika 6 (74) (2008) 11–16.

[17] K. Ariza-Zafra, R.J. Berry, M.S.A. Bradley, Review of models for predicting the discharge rates of bulk particulates from silos and bins, in: Proceedings – RELPOWFLO IV, pp. 492–499. Tromsø (2008).

[18] R. Balevičius, A. Džiugys, R. Kačianauskas, Discrete element method and its application to the analysis of penetration into granular media, Journal of Civil Engineering and Management 10 (1) (2004) 3–14.

[19] R. Balevičius, R. Kačianauskas, Z. Mróz, I. Sielamowicz, Discrete-particle investigation of friction effect in filling and unsteady/steady discharge in three-dimensional wedge-shaped hopper, Powder Technology 187 (2008) 159–174.

[20] R. Balevičius, R. Kačianauskas, A. Džiugys, A. Maknickas, V. Vislavičius, DEMMAT code for numerical simulation of multi-particle dynamics, Information Technology and Control 34 (1) (2005) 71–78.

[21] R. Balevičius, R. Kačianauskas, A. Džiugys, A. Maknickas, K. Vislavičius, Investigation of performance of programming approaches and languages used for numerical simulation of granular material by the discrete element method, Computer Physics Communications 175 (6) (2006) 404–415.

[22] P.A. Langston, U. Tüzün, D.M. Heyes, Continuous potential discrete particle simulations of stress and velocity fields in hoppers: transition from fluid to granular flow, Chemical Engineering Science 49 (8) (1994) 1259–1275.

[23] P.A. Langston, U. Tüzün, D.M. Heyes, Discrete element simulation of granular flow in 2D and 3D hoppers: dependence of discharge rate and wall stress on particle interactions, Chemical Engineering Science 50 (6) (1995) 967–987.

[24] R. Balevičius, R. Kačianauskas, Z. Mroz, I. Sielamowicz, Microscopic and macroscopic analysis of granular material behaviour in 3D flat-bottomed hopper by the discrete element method, Archives of Mechanics 59 (3) (2007) 231–257.

[25] R.M. Nedderman, Statics and kinematics of granular materials, Cambridge University Press, New York, 1992.

[26] O. Pouliquen, R. Gutfraind, Stress fluctuations and shear zones in quasi-static granular chute flows, Phys. Rev. E 53 (1996) 557–561.

[27] D. Tabor, The mechanism of rolling friction. I. The plastic range, Proceedings of the Royal Society of London. Series A, Mathematical and Physical Sciences 229 (1177) (1955) 181–1998.

[28] D. Tabor, The mechanism of rolling friction. II. The elastic range, Proceedings of the Royal Society of London. Series A, Mathematical and Physical Sciences 229 (1177) (1955) 198–220.

[29] C. Zhou, J.Y. Ooi, Numerical investigation of progressive development of granular pile with spherical and non-spherical particles, Journal of Mechanics of Materials 41 (6) (2009) 707–714.

[30] J. Ai, J.-F. Chen, J.M. Rotter, J.Y. Ooi, Assessment of rolling resistance models in discrete element simulations, 2010. 10.1016/j.powtec.2010.09.030.

[31] Y.C. Zhou, B.D. Wright, R.Y. Yang, B.H. Xu, A.B. Yu, Rolling friction in the dynamic simulation of sand pile formation, Physica A 269 (1999) 536–553.

[32] K. Iwashita, M. Oda, Micro-deformation mechanism of shear banding process based on modified distinct element method, Powder Technology 109 (2000) 192–205.

[33] H.P. Zhu, A.B. Yu, A theoretical analysis of the force models in discrete element method, Powder Technology 161 (2006) 122–129.

[34] W.R. Ketterhagen, R. Bharadwaj, B.C. Hancock, The coefficient of rolling resistance (CoRR) of some pharmaceutical tablets, International Journal of Pharmaceutics 392 (2010) 107–110.

[35] J. Łukaszuk, M. Molenda, J. Horabik, J. Wiącek, Method of measurement of coefficient of friction between pairs of metallic and organic objects, Acta Agrophysica 13 (2) (2009) 407–418.

[36] J. Horabik, M. Molenda, Physical properties of granular food materials, Acta Agrophysica 74 (2002) 1–89.

[37] R. Balevičius, I. Sielamowicz, Z. Mroz, R. Kačianauskas, Analysis and simulation of granular material flow patterns in silo model, in: Proceedings of World Congress on Particle Technology WCPT-6, CD-ROM, pp. 1–5. Nuremberg (2010).

[38] R. Balevičius, R. Kačianauskas, Z. Mroz, I. Sielamowicz, Comparison of wall pressures measured in the model silo with DEM simulation, in: 36th Solid Mechanics Conference. Selected topics of contemporary solid mechanics – IFTR reports, pp. 220–221. Gdansk (2008).

[39] Y. Yu, H. Saxén, Discrete element method simulation of properties of a 3D conical hopper with mono-sized spheres, Advanced Powder Technology (2010), doi:10.1016/j.apt.2010.04.003.

[40] J. Choi, A. Kudrolli, M. Bazant, Velocity profile of granular flows inside silos and hoppers, Journal of Physics Condensed Matter 17 (2005) S2533–S2548.

[41] A. Medina, J.A. Córdova, E. Luna, C. Treviño, Velocity field measurements in granular gravity flow in a near 2D silo, Physics Letters A 250 (1998) 111–116.

[42] J. Litwiniszyn, The model of a random walk of particles adopted to researches on problem of mechanics of loose media, Bulletin l'Academie Polonaise Sciences 9 (1963) 61–70.

[43] W.W. Mullins, Critique and comparison of two stochastic theories of gravity-induced particle flow, Powder Technology 23 (1979) 115–119.

[44] K. D. Kafui, C. Thornton, Some observations on granular flow in hoppers an silos, Powders and Grains 97, Durham (1997) 511–514.

[45] C.S. Chou, J.Y. Hsu, Kinematic model for granular flow in a two-dimensional flat-bottomed hopper, Advanced Powder Technology 14 (3) (2003) 313–331.